Adaptive STFT for UAV Micro-Doppler Signature Analysis

Daniel Herr, Dave Tahmoush

University of Kansas

Lawrence, KS, USA

ABSTRACT

This paper adapts the general form of the Short-Time Fourier Transform by including an adaptive Gaussian window to enable more consistent UAV micro-Doppler analysis. Developing a technique for selecting an appropriate time-window for the STFT enables the maximization of the separability of relevant features for micro-Doppler analysis. This is approached in the context of UAV rotor blade analysis. Techniques for estimating the periodicity of the radar returns as well as examining the temporal correlation of the signal are presented. Simulated and experimental results are provided showing the efficacy of the adaptive STFT algorithm for producing more consistent micro-Doppler signatures.

I. INTRODUCTION

The increased use and widespread availability of commercial UAVs has driven demand for techniques for UAV detection and classification. A significant challenge to this aim is the relatively low radar cross-section (RCS) and slow speeds that these UAVs tend to move. These attributes lead to the increased potential for false alarms due to low SNR and potential confusers such as birds [1]. Previous research has shown that the distinctive micro-Doppler signatures of UAVs are an effective input into classifiers and dissimilators designed for detecting UAVs [1, 2].

Micro-Doppler blade lines have been shown to be an effective way to classify UAVS [2] and separate them from clutter [3]. UAV micro-Doppler plots showing HERM line phenomenology have been shown effective at differentiating between loaded/ unloaded UAVs [1]. UAVs exhibiting HERM line micro-Doppler signatures has been shown as a way to differentiate between UAVs and birds [4].

The same data can be used to generate spectrograms showing blade flash or HERM line phenomenology as long as there is enough sample support for the blade flashes. We can see this in this paper [5] where they used the same data to make spectrograms showing both phenomena.

HERM lines and blade flashes are discussed in [6] where the relationship between STFT window length and blade flash and HERM line phenomenology is discussed. Micro-Doppler signatures for several UAVs and birds are studied [7]; the distinct UAV micro-Doppler features such as the blade flash and HERM lines are good ways to differentiate UAVs from birds.

The motivation for an adaptive Gaussian window STFT is to provide more consistent micro-Doppler signatures for feature extraction and classifier inputs. This may increase the stability of micro-Doppler signatures across platforms and across different targets moving at different speeds. A practical motivation for this paper is consistent UAV detection and recognition by creating more consistent data products for feature extraction and classifier inputs.

II. HERM LINE PHENOMENOLOGY

In [6] we see that HERM line or blade flash phenomenology is related to the STFT window time width. We wish to further address this phenomenon. The standard form of the STFT is given as

$$STFT\left(t,f\right)=\int_{-\infty}^{+\infty}x\left(t\right)w\left(t-\tau\right)e^{-j\omega t}dt$$

Where a spectrogram is generated as

$$SPECTROGRAM\left\{t,f\right\}=\left|STFT\left(t,f\right)\right|^{2}$$

The STFT applies a sliding window across an input signal and then takes the Fourier transform at each time t. The time-width of this window function determines the instantaneous frequency resolution of the resulting spectrogram. Also, the intuition and knowledge we have about the Fourier transform can be applied to the instantaneous frequency calculated by the STFT. Primarily, if the input signal is a time-periodic signal with many periods within a single window function we expect to see a discretized version of the power spectrum of a single period of the waveform. The idealized case of a stationary rotor blade rotating at a constant velocity presents such a signal.

This effect has been examined in the case of helicopters and their related micro-Doppler signatures. The spectrograms of a constantly rotating helicopter blades often present continuous discretized lines in the doppler domain. These lines have been termed Helicopter Rotor Modulation (HERM) lines. For additional information on HERM lines and rotor blade returns see references in [8] and [9].

The (Helicopter Rotor Modulation) HERM line or blade line phenomenology is created by the short-time Fourier transform (STFT) of time-periodic signals like blade flashes. We consider the case of two different Gaussian windows used to analyze the same return signal from a simulated rotating blade shown in Figure 1. The first window is sized such that 0.5 periods of the time-periodic blade return signal lies within the window's approximate time-extent; noted as $N_{p,win}=0.5$ (number of signal periods per window time-width). The second window is sized such that 6.0 periods of the time-periodic blade return signal lies within the window's approximate time-extent ($N_{p,win}=6.0$).

The Fourier Transform is taken of each windowed signal and one slice of the each STFT is calculated. This process is repeated for each shifted time-window. We see the blade flash phenomenology in the case where the window is small relative to the period of the blade return signal (Figure 2). This makes sense as the windowed signal can vary dramatically as the window moves across a single period of the blade return signal.

We see the HERM line phenomenology in the case where the window is large relative to the period of the blade return signal (Figure 3). In this case shifting the window along the blade-return signal does not result

in a significantly different spectrum. For the case where the window is large relative to the period of the blade return signal we see that the HERM line phenomenology is dominant.

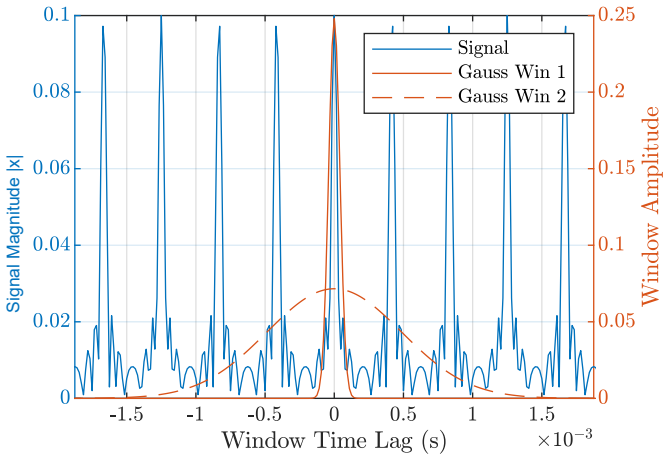

Figure 1: Plot showing the simulated return from a rotating blade of constant frequency. Two Gaussian windows of differing width are shown.

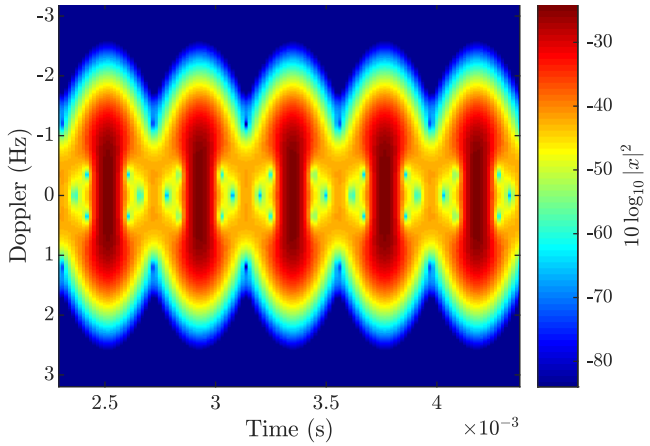

Figure 2: Micro-Doppler signature of rotating blades. Here $N_{p,win} = 0.5$

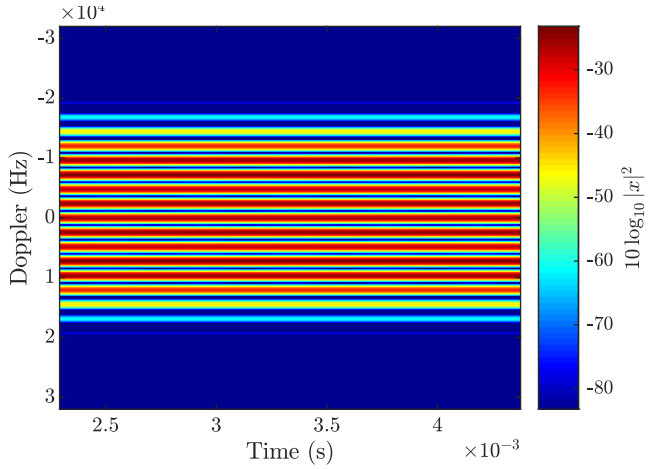

Figure 3: Micro-Doppler signature of rotating blades.
The time scale was set to be equal to t_{win}. Here $N_{p,win} = 6.0$

Based on these observations we define rough qualitative regions to predict which phenomena will be dominate. We define a region where the blade flash phenomenology dominates as:

$$R_{FLASH}(N_{p,win}) \in \{N_{p,win} \mid N_{p,win} < 1.0\}$$

We define a region where the HERM line phenomenology dominates as:

$$R_{HERM}(N_{p,win}) \in \{N_{p,win} \mid N_{p,win} > 3.0\}$$

III. ADAPTIVE GAUSSIAN WINDOW STFT

An adaptive STFT is presented in [10], where the "concentration" of the spectrogram is maximized at each time sample. This paper adapts the general form of the STFT:

$$STFT(t,f) = \int_{-\infty}^{+\infty} x(t)\, w(t,\tau)\, e^{-j\omega t}\, dt$$

by including an adaptive gaussian window. The Gabor transform is the STFT using a Gaussian window and it has the minimal product of time resolution and frequency resolution [8]. Here we consider a generalized form of the STFT, where an adaptive Gaussian window is allowed to change as a function of delay.

$$w(t,\tau) = \frac{1}{\sqrt{2\pi\sigma(\tau)}} \exp\left\{-\frac{(t-\tau)^2}{2\sigma(\tau)}\right\}$$

The proposed algorithm adjusts the variance of the window function based on the estimated instantaneous periodicity.

We approximate the extent of our gaussian window as the time-width that contains some percentage of the area of the window. Here γ represents the percent of the window area expressed from 0 to 1. For these simulations a value of 0.99 was used. We then use the Gaussian right-tailed probability function, $\mathrm{Q}^{-1}(x)$, to calculate the approximate window time-width.

$$t_{win} \approx 2\sigma\, \mathrm{Q}^{-1}\left(\frac{1-\gamma}{2}\right) t_s$$

Where t_s corresponds to the sample period of the STFT dimension.

We specify a user defined parameter $N_{p,win}$ which specifies the real number of fundamental periods of the micro-Doppler return per window. Here we express $\hat{t}_p(\tau)$ the instantaneous estimated fundamental periodicity.

$$N_{p,win} = \frac{t_{win}}{\hat{t}_p(\tau)} = \frac{2\sigma(\tau)\,\mathrm{Q}^{-1}\left(\frac{1-\gamma}{2}\right) t_s}{\hat{t}_p(\tau)}$$

We then express $\sigma(\tau)$ as a function of $\hat{t}_p(\tau)$

$$\sigma(\tau) = \frac{N_{p,win}\hat{t}_p(\tau)}{2Q^{-1}\left(\frac{1-\gamma}{2}\right)t_s}$$

In order for the adaptive STFT function to perform well, we must have an accurate estimate of the instantaneous fundamental period of the micro-Doppler signal. There are many viable techniques such as the STFT, Cepstral analysis, Wigner-Ville Distribution and the Spectral Correlation Function, etc. Here we perform peak detection on the 2D-FFT of the sample correlation matrix (SCM). This method provides an SNR gain over simply taking the Fourier transform of the slice so long as the process remains approximately WSS over the slice.

We define a snapshot matrix of our input signal $\mathbf{x}$ as

$$\mathbf{x}(n) = \begin{bmatrix} x(n) & x(n-1) & \ldots & x(n-M+1) \end{bmatrix}^T$$

We estimate the instantaneous SCM using N slices of $\mathbf{x}$ [11]

$$\hat{\mathbf{R}} = \frac{1}{N}\sum_{n=1}^{N}\mathbf{x}(n)\mathbf{x}^H(n)$$

And then determine the 2D FFT

$$\hat{\mathbf{R}}_f = \mathbf{A}\hat{\mathbf{R}}\mathbf{A}^H$$

Where $\mathbf{A}$ is the DFT matrix.

$$\hat{\mathbf{r}}_f = \mathrm{diag}\left(\hat{\mathbf{R}}_f\right)$$

Perform peak detect on

$$\mathbf{s}_f = \left|\mathbf{r}_f\right|^2$$

We then extract an estimate $\hat{f}_p$

$$\hat{t}_p = \frac{1}{\hat{f}_p}$$

IV. SIMULATION RESULTS

Simulation of an idealized rotor blade was performed using the simulation released in [8]. The simulation is performed using the quasi-static approximation where the objects are considered static during each time instant and then move between samples. The blades were modeled as a continuous series of point scatters that extended over the length of the blade. Effects due to non-rigid motion were ignored as were effects due to non-uniform blades. Similar effects on measured data are shown in Section V [12].

The simulation in Section I shows that for a constant rotation rate we can generate a spectrogram showing HERM line or blade flash phenomenology based on the choice of window size given a high enough sample rate. Once we have obtained an estimate of the rotational frequency, we can calculate a window size that will demonstrate either phenomenon.

Figure 5 shows that as the rotation rate of the blades increase, the observable phenomenology in the system changes if we use a constant window size. At slower rotation rates (early in Figure 5), the blade flash phenomenology is clear. At much faster rotation rates (late in Figure 5), the HERM line phenomenology is clear. There is an intermediate area where both phenomenologies have aspects that are visible. This change in phenomenology can make feature extraction challenging and can affect the ability to classify the targets.

The application of an adaptive Gaussian window is shown in Figure 6. As the rotational rate of the rotor increases, the STFT window size is reduced at a commensurate rate as shown in Figure 12. Here, the adaptive Gaussian window produces the blade flash phenomenon for the duration of the simulation Figure 10. The tradeoff here is that while the spectrogram maintains a single phenomenology, the frequency resolution is inversely related to the STFT window time-width. Hence the frequency resolution is degraded as the rotor blade speed increases.

We can also approach this simulation with the goal of maintaining the HERM line phenomenology. Figure 11 shows a spectrogram generated from a STFT using an adaptive Gaussian window with a target of 6 signal periods per window length. Here HERM line phenomenology is maintained through then entire spectrogram. The trade-off with a larger window size is that the signal must remain relatively stationary over the STFT window length or the HERM line phenomena will become muddled. So we must consider the time-width that the signal remains temporally correlated. The selection of spectrogram phenomena is trivial given that the signal is indeed periodic and an accurate estimate of this periodicity is available.

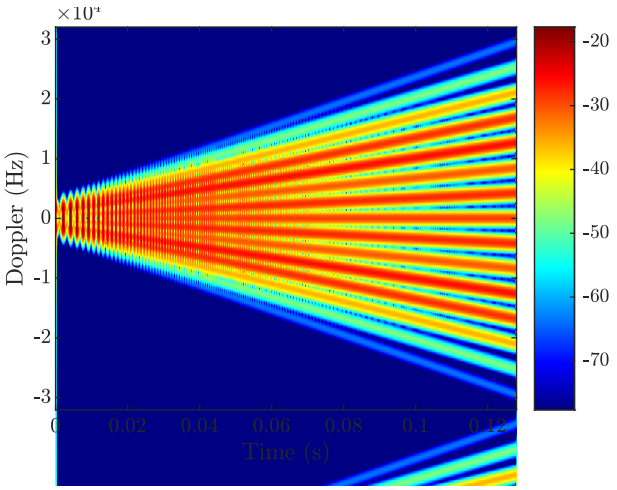

Figure 4: Simulated Micro-Doppler signature for linearly accelerating rotor blade. Fixed Gaussian window with $\sigma = 16$

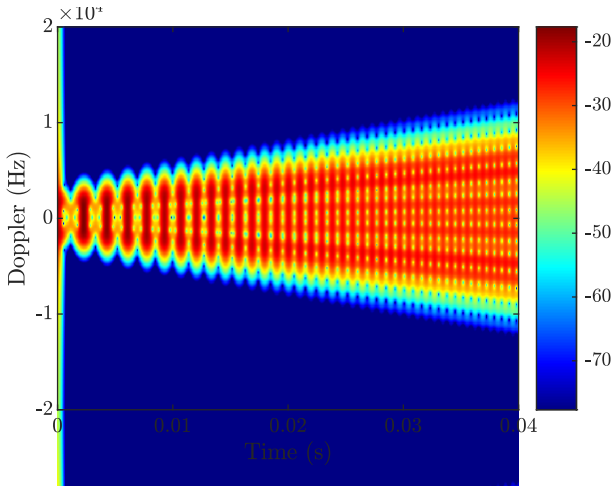

Figure 5: Simulated Micro-Doppler signature for linearly accelerating rotor blade. Fixed Gaussian Window

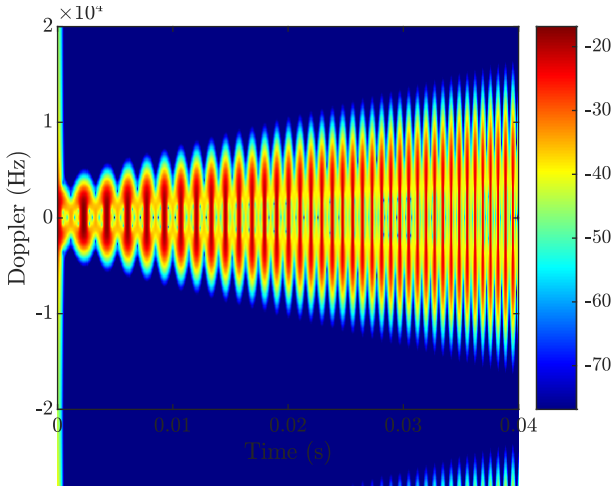

Figure 6: Simulated Micro-Doppler signature for linearly accelerating rotor blade. Adaptive Gaussian Window

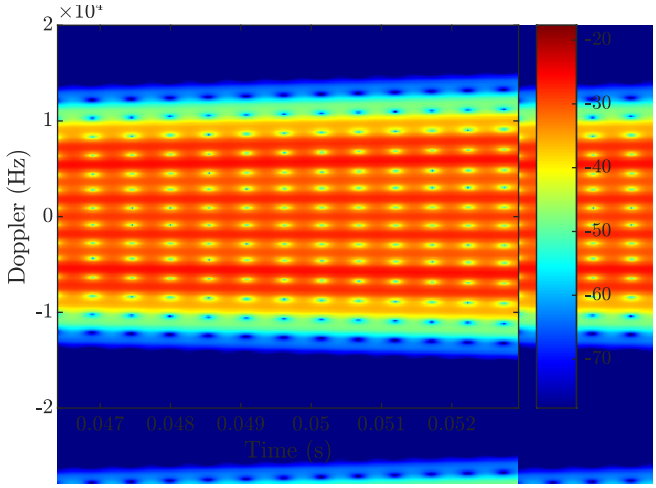

Figure 7 Simulated Micro-Doppler signature for linearly accelerating rotor blade. Fixed Gaussian Window, Indeterminate region.

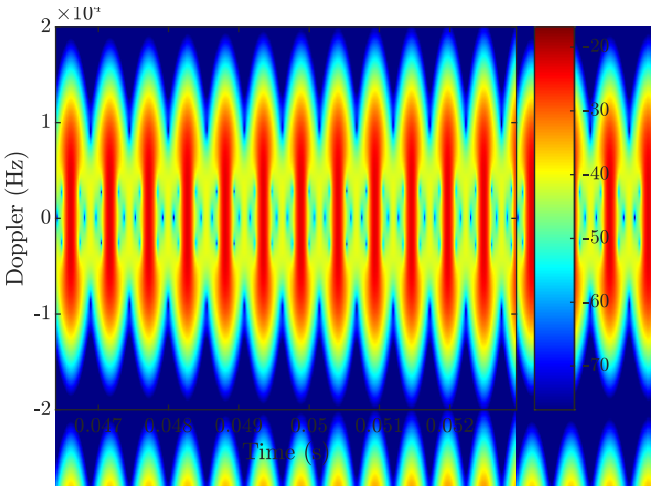

Figure 8: Simulated Micro-Doppler signature for linearly accelerating rotor blade. Adaptive Gaussian Window, Indeterminate region.

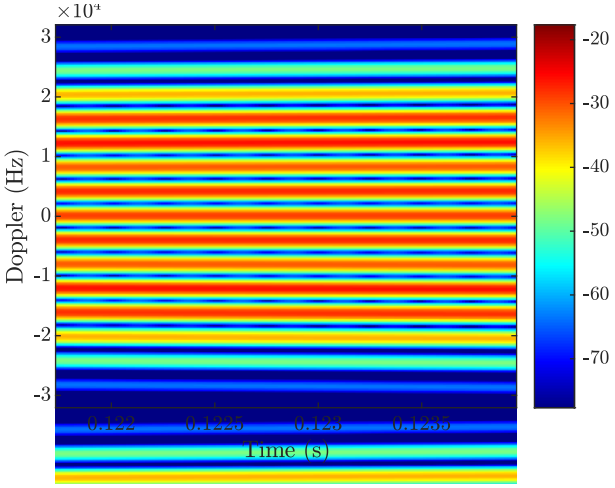

Figure 9: Simulated Micro-Doppler signature for linearly accelerating rotor blade. Fixed Gaussian Window, HERM line region.

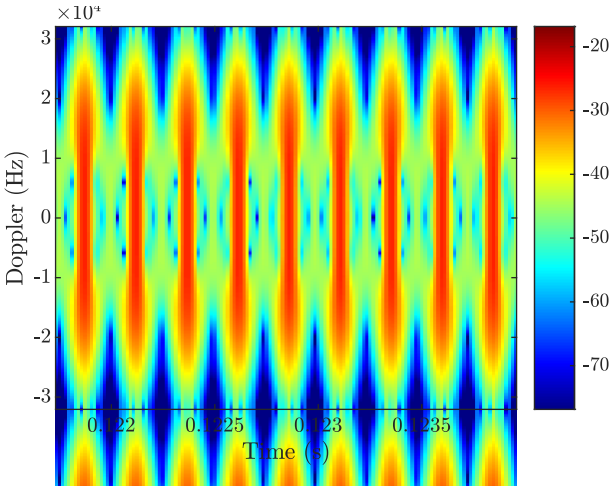

Figure 10: Simulated Micro-Doppler signature for linearly accelerating rotor blade. Adaptive Gaussian Window, HERM line region.

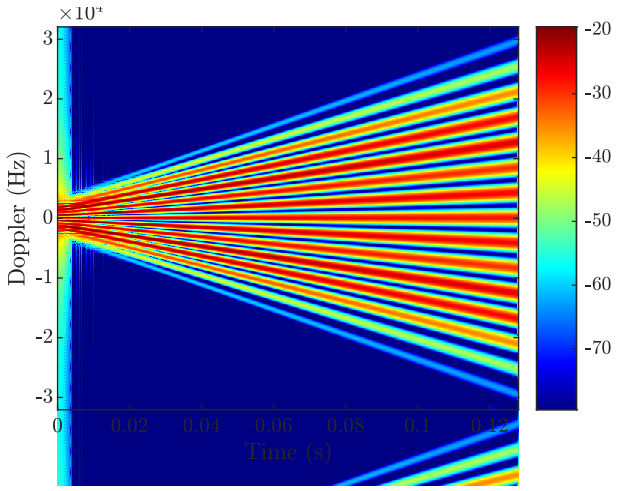

Figure 11: Simulated Micro-Doppler signature for linearly accelerating rotor blade. Adaptive Gaussian Window, set to $N_{p,win} = 6.0$

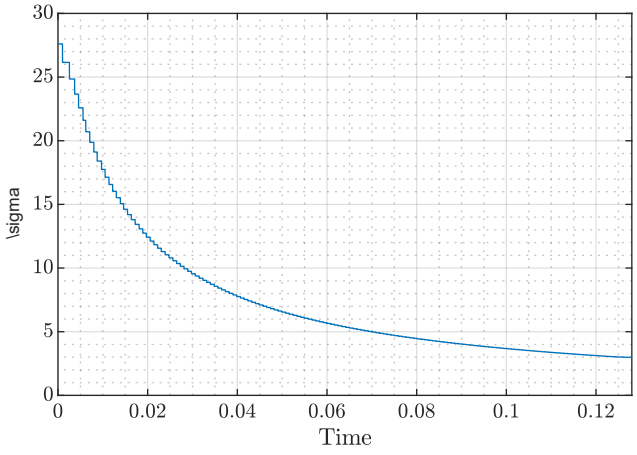

Figure 12: Adaptive Gaussian window size vs time.

V. EXPERIMENTAL RESULTS

Experimental results were obtained using a radar system from the MIT Build a Radar project [13]. The system is an FMCW radar operating at 2.4 GHz with up to 80 MHz of signal bandwidth. The system employs stretch processing and achieves a sample-rate of 40 kHz (single-channel). The system was operated in CW mode and was used to illuminate a single rotor from a UAV. This setup highlights the ability to apply micro-Doppler analysis to low-cost radar hardware.

The MIT Build a Radar was used to illuminate a single UAV rotor secured to a test bench. The rotor was setup to rotate at a constant rate in an otherwise static scene. A spectrogram was created using a STFT with a relatively wide STFT window (shown in Figure 13). Here, the HERM line phenomenology is clearly visible. Next the adaptive STFT was applied to the data with a setting of 0.5 signal periods per window and the spectrogram in Figure 14 was generated. Here the blade flash phenomenon is clearly visible. For the case of a constant RPM we could generate the same plot using an appropriately sized STFT width;

however, here the size of the window is automatically determined based on the underlying signal structure.

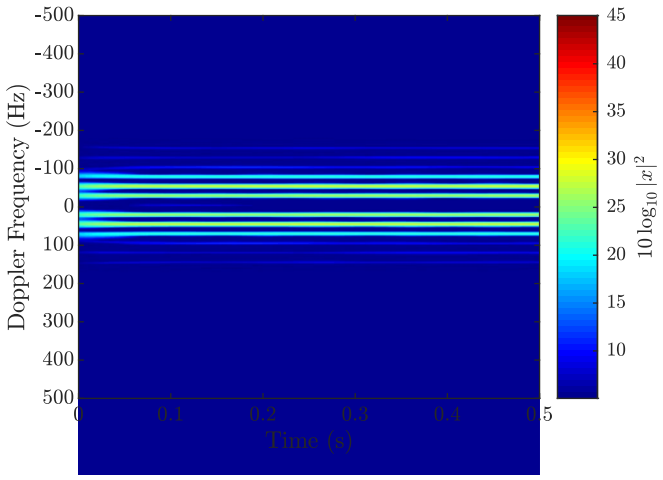

Figure 13: Micro-Doppler signature of BladeR2_fast.mat using static Gaussian window with $\sigma = 85$. Corresponds to ~6 flashes per window.

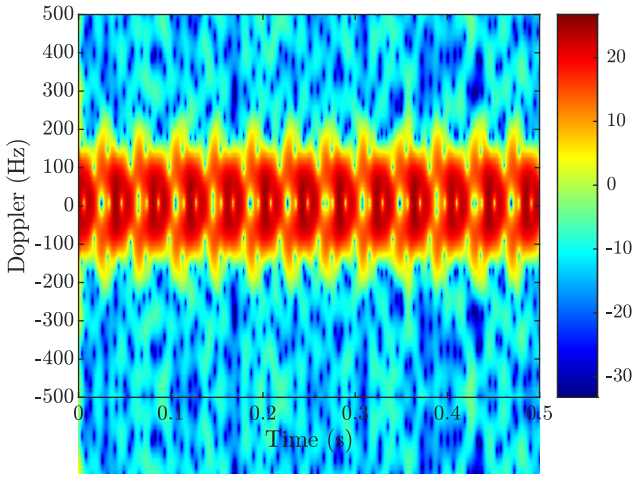

Figure 14: Micro-Doppler signature of BladeR2_fast.mat using adaptive Gaussian window. $\sigma \approx 7.8$

Next the rotor blade was configured to vary its speed with time. The blade started with no rotational movement, was accelerated to a peak speed, and then decelerated and returned to no rotational movement. Again, the radar was operated in CW mode and illuminated the rotor blade in an otherwise static scene. A spectrogram of the received data is shown in Figure 15. HERM lines are clearly visible, and the state of the rotor blade readily determined. Next, the rotational rate of the blade was estimated in Figure 21 and used to generated adaptive STFTs. A adaptive STFT was applied to the data with a target of 0.5 signal periods per STFT window and the results plotted in Figure 16, Figure 18, and Figure 20. Comparing these plots to their constant window STFT counterparts show that a consistent blade flash phenomenology is maintained despite the increasing rotor speed. Of particular interest is where the STFT is producing clear blade flashes yet the constant STFT is producing an intermediate response.

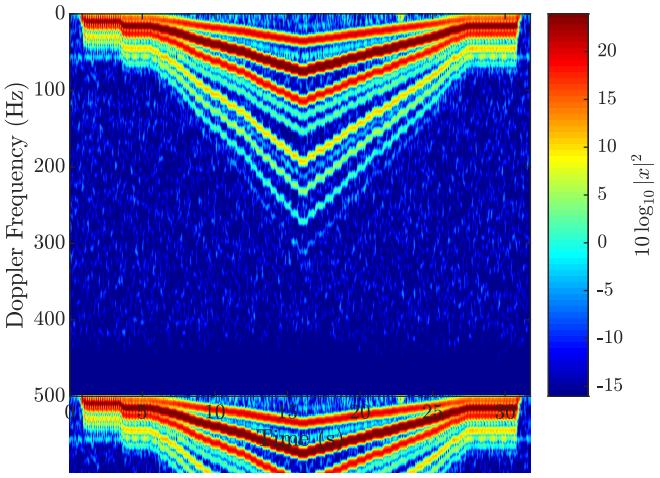

Figure 15: Micro-Doppler signature using STFT with $\sigma = 42.6$

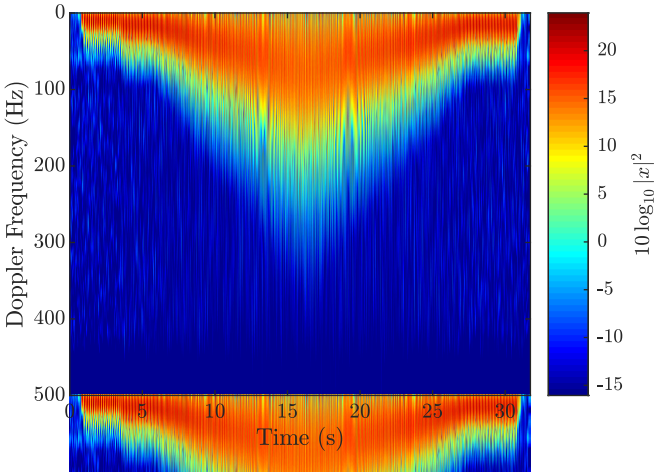

Figure 16: Micro-Doppler Signature using Adaptive STFT

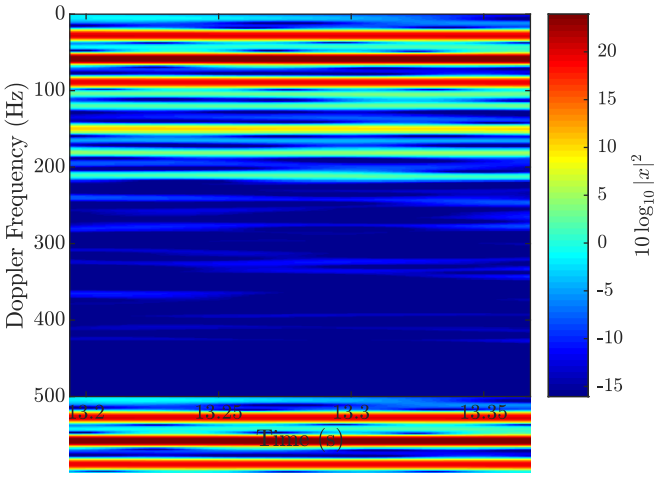

Figure 17: Micro-Doppler signature using STFT with $\sigma = 42.6$

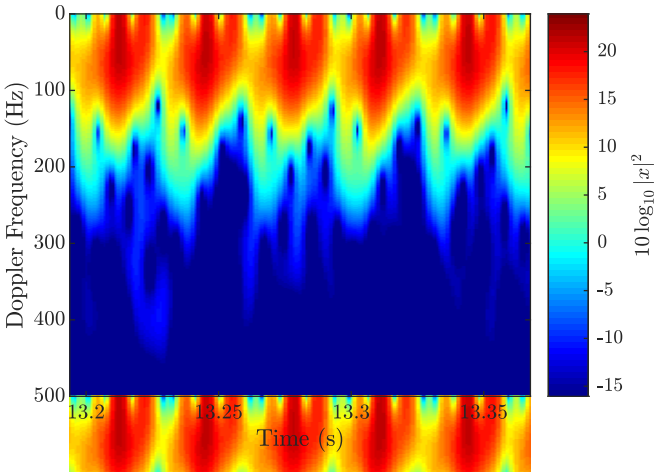

Figure 18: Micro-Doppler Signature using Adaptive STFT

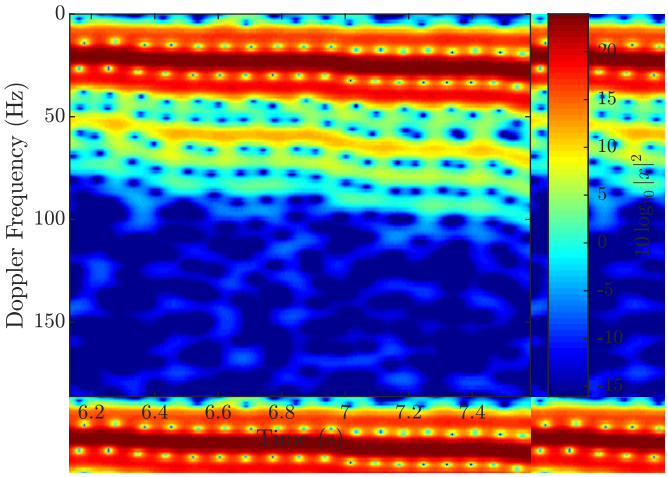

Figure 19: Micro-Doppler Signature using STFT with $\sigma = 42.6$

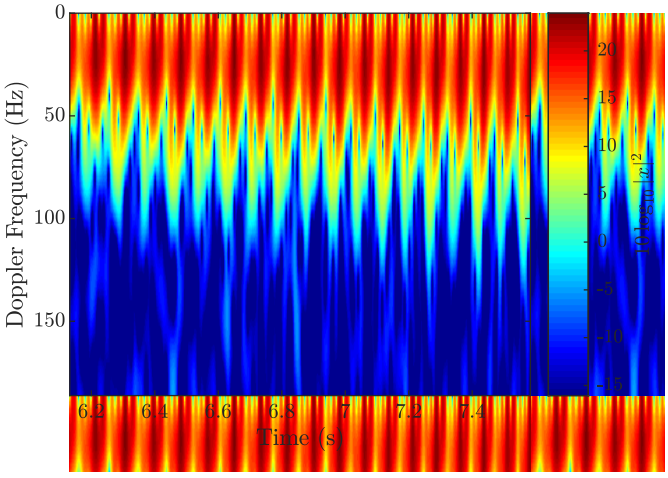

Figure 20: Micro-Doppler Signature using Adaptive STFT

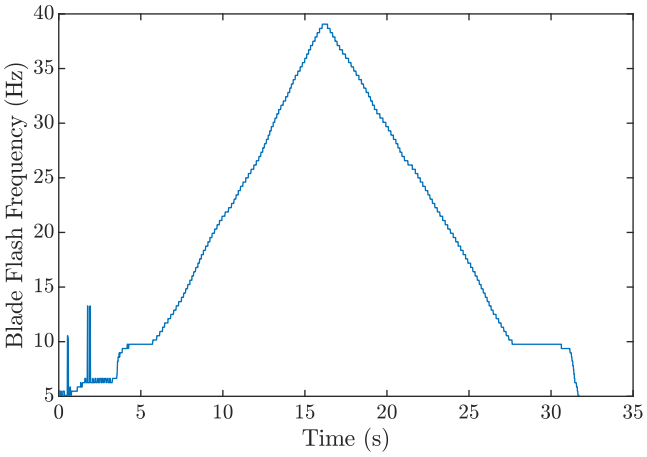

Figure 21: Fundamental Frequency estimated using SCM Method

VI. CONCLUSION

This paper addresses the concepts of HERM line and blade flash phenomena and presents a method to produce more consistent spectrograms. The present work adapts the general form of the STFT to allow for adaptation of the STFT window size in response to the instantaneous signal structure. The efficacy of this algorithm was shown using both simulated and experimental data of a rotating UAV blade. The algorithm was show effective at producing consistent spectrograms for the case of singular rotating blades with constant or variable speeds. In addition, the ability to convert from blade flash to HERM line phenomenology should allow multiple different classification algorithms to be used on the same data more consistently.

Future work should extend the simulations and experimental results to include multi-rotor scenarios such as multi-rotor UAVs. Additional techniques for estimating the signal periodicity should be explored as the algorithm is only as effective as the estimate of rotational period. Also, the work could be extended to include multiple STFT window types and the determination of stricter bounds on the blade flash and HERM line phenomenology regions. Also, could show test the efficacy of classifiers using the adaptive STFT vs constant window STFT.

REFERENCES

[1] M. Ritchie, F. Fioranelli, H. Borrion, and H. Griffiths, "Multistatic micro-Doppler radar feature extraction for classification of unloaded/loaded micro-drones," *IET Radar, Sonar & Navigation,* vol. 11, no. 1, pp. 116-124, 2017.

[2] M. Ritchie, F. Fioranelli, H. Griffiths, and B. Torvik, "Micro-drone RCS analysis," in *2015 IEEE Radar Conference*, 2015, pp. 452-456.

[3] F. Hoffmann, M. Ritchie, F. Fioranelli, A. Charlish, and H. Griffiths, "Micro-Doppler based detection and tracking of UAVs with multistatic radar," in *2016 IEEE Radar Conference (RadarConf)*, 2016, pp. 1-6.

[4] M. Ritchie, F. Fioranelli, H. Griffiths, and B. Torvik, "Monostatic and bistatic radar measurements of birds and micro-drone," in *2016 IEEE Radar Conference (RadarConf)*, 2016, pp. 1-5.

[5] J. J. M. d. Wit, R. I. A. Harmanny, and G. Prémel-Cabic, "Micro-Doppler analysis of small UAVs," in *2012 9th European Radar Conference*, 2012, pp. 210-213.

[6] S. Rahman and D. A. Robertson, "Millimeter-wave micro-Doppler measurements of small UAVs," in *SPIE Defense + Security*, 2017, vol. 10188: SPIE.

[7] S. Rahman and D. A. Robertson, "Radar micro-Doppler signatures of drones and birds at K-band and W-band," *Scientific Reports,* vol. 8, no. 1, p. 17396, 2018/11/26 2018.

[8] V. C. Chen, *The micro-Doppler effect in radar*, Second edition. ed. (Artech House radar series). Norwood, MA: Artech House, 2019, pp. xv, 341 pages.

[9] V. C. Chen, D. Tahmoush, and W. J. Miceli, *Radar micro-Doppler signatures : processing and applications* (IET radar, sonar and navigation series, no. volume 34). Stevenage: Institution of Engineering and Technology, 2014, pp. xii, 394 pages.

[10] B. Boashash, *Time-frequency signal analysis and processing : a comprehensive reference*, Second edition. ed. (EURASIP and Academic Press series in signal and image processing). 2016, pp. xlvii, 1020 pages.

[11] S. S. Haykin, *Adaptive filter theory*, Fifth edition. ed. Upper Saddle River, New Jersey: Pearson, 2014, pp. xvii, 889 pages.

[12] D. Tahmoush, "Review of micro-Doppler signatures," *IET Radar, Sonar & Navigation,* vol. 9, no. 9, pp. 1140-1146, 2015.

[13] K. E. Kolodziej *et al.*, "Build-a-Radar Self-Paced Massive Open Online Course (MOOC)," in *2019 IEEE Radar Conference (RadarConf)*, 2019, pp. 1-5.